analytical chemistry

pubs.acs.org/ac

Letter

# Ratiometric pH-Responsive $^{19}$F Magnetic Resonance Imaging Contrast Agents Based on Hydrazone Switches

Dawid Janasik, Krzysztof Jasiński, Władysław P. Węglarz, Ivan Nemec, Pawel Jewula, and Tomasz Krawczyk*

Cite This: *Anal. Chem.* 2022, 94, 3427−3431

Read Online

ACCESS | Metrics & More | Article Recommendations | Supporting Information

**ABSTRACT:** Hydrazone-based molecular switches serve as efficient ratiometric pH-sensitive agents that can be tracked with $^{19}$F NMR/MRI and $^{1}$H NMR. Structural changes induced between pH 3 and 4 lead to signal appearance and disappearance at $^{1}$H and $^{19}$F NMR spectra allowing ratiometric pH measurements. The most pronounced are resonances of the $CF_3$ group shifted by 1.8 ppm with $^{19}$F NMR and a hydrazone proton shifted by 2 ppm with $^{1}$H NMR.

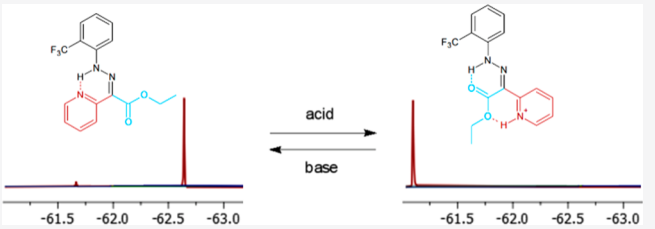




The measurement of pH is a fundamental aspect of chemical research. Many tools have been developed for this purpose, and visual indicators[1] and pH-sensitive electrodes[2] are commonplace in almost every laboratory. More sophisticated techniques were proposed for medicinal diagnostic, where a deviation from physiological pH indicates various pathological changes. For example, gastroesophageal reflux disease manifests an esophageal pH < 4[3,4] while solid tumors are more acidic (pH 6.2−7.0) than normal tissue (pH ∼ 7.5).[5,6] Very low pH is also observed during cellular studies of lysosomes 4.0−5.0.[7,8] The procedures used for pH measurements in medicine rely on microelectrodes and several imaging techniques such as electron paramagnetic resonance (EPR), positron emission tomography (PET), photoacoustic imaging (PAI), and magnetic resonance imaging (MRI).[9]

MRI is a noninvasive diagnostic tool for soft tissues that uses the magnetic properties of the $^{1}$H nucleus. It is one of the most widely used imaging procedures in medicine and offers excellent spatial resolution and unlimited penetration depth and provides knowledge that cannot be accessed by other means.[10,11] In order to improve the quality of the images, $^{19}$F MRI has been extensively investigated as a complementary modality that allows so-called hot spot imaging.[12,13] Since $^{19}$F atoms are not present in soft tissues, this modality allows for the accurate representation of the targeted organ without background signals; however, it requires the introduction of an appropriate contrast agent containing $^{19}$F nuclei into the organism.[14]

Regarding the $^{19}$F NMR or MRI as an aid in pH measurements, several molecular probes have been developed. The earliest reports concerned fluorinated aniline derivatives, whose mechanism of action was based on protonation of the aniline nitrogen, which changed the chemical shift of the fluorine atom.[15−17] Other concepts utilized PEGylated nanogels containing perfluorocarbons,[18] $C_6F_6$-loaded Au-fluorescent mesoporous silica nanoparticles,[19] or copolymers.[20−23] In those cases, the mechanism of pH-depended signal changes was either based on the reversible volume phase transition of the nanogel, which emitted an $^{19}$F NMR signal, or the irreversible decomposition of the capsule under the influence of pH and the release of fluoroorganic groups, respectively.[24] In each case, a single $^{19}$F signal with a pH-dependent chemical shift was observed. A probe displaying two separate signals with pH-dependent integral ratios (allowing internal reference and ratiometric measurements) would be more convenient for diagnostic purposes.

Hydrazone-based molecular switches could be used in such a role. Molecular switches are usually defined as molecules that can reversibly transform between two (or more) thermodynamically stable states.[25,26] Such compounds are sensitive to external stimuli such as light, pH, or electric current and include photochromic switches, host−guest switches, and rotaxanes.[27−29] The main applications of molecular switches is expected to include molecular electronics (high-density data storage) or organic diodes.[30] They have been also reported as chemosensors or fluorescence imaging agents.[31,32]

Here, we demonstrate the first application of ratiometric reversible hydrazone-based molecular switches as $^{19}$F NMR/MRI pH-responsive compounds based on chemical shift changes.

**Received:** November 16, 2021
**Accepted:** February 10, 2022
**Published:** February 14, 2022





https://doi.org/10.1021/acs.analchem.1c04978
*Anal. Chem.* 2022, 94, 3427−3431

The structures (Figure 1) were derived from Aprahamian's hydrazone switch.[33] The synthesis of hydrazones **1**-*E*, **2**-*E*, and

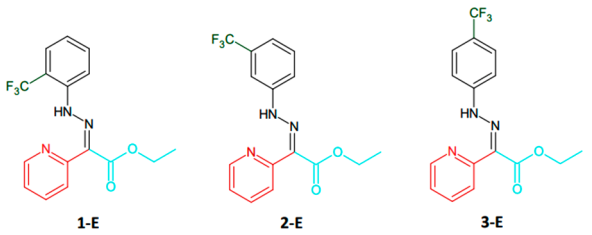


**Figure 1.** Chemical structures of fluorinated hydrazones.

**3**-*E* involved coupling trifluoromethylanilines with ethyl pyridyl-acetate.[34] Briefly, trifluoromethylaniline in EtOH was treated with concentrated HCl and then $NaNO_2$ at 0 °C to give trifluoromethyl-1-benzenediazonium chloride. In a separate flask, ethyl-2-pyridyl-acetate was treated at 0 °C with sodium acetate in EtOH−$H_2O$ (8:1). These two solutions were combined and stirred at 0 °C for 1 h and then overnight at RT. The resultant reaction mixture was washed with methylene chloride, and the organic fraction was washed twice with saturated sodium bicarbonate solution and dried over magnesium sulfate. The crude product was subjected to column chromatography ($SiO_2$, $CH_2Cl_2$−MeOH, 8:1) to give pure compounds as an orange solid (yields, 55−65%).

According to X-ray crystallography, the structures were nearly planar, and H-bonding between the N−H proton and the pyridine nitrogen subunit was observed (Figure S13). The $^1$H NMR spectra of molecular switches (Figure 2) in $CD_3CN$ showed a characteristic H-bonded N−H resonance around 15 ppm, in addition to the expected aromatic and aliphatic signals.

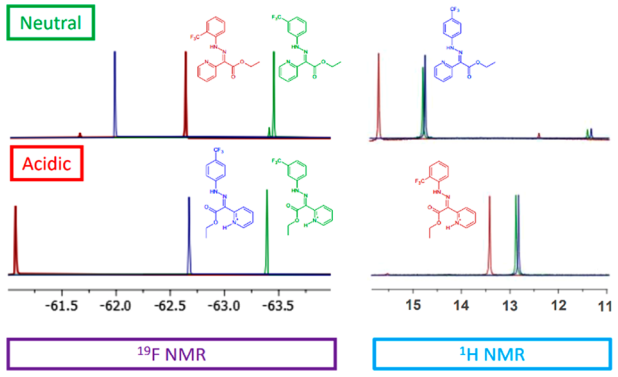


**Figure 2.** $^{19}$F NMR (left) and $^1$H NMR (right) spectra (400 MHz) in $CD_3CN$; (top) **1**-*E* (red), **2**-*E* (green), and **3**-*E* (blue); (bottom) *Z*-$H^+$ recorded after the addition of 1.6 equiv of trifluoroacetic acid (TFA).

The N−H chemical shift indicates that the pyridine nitrogen is H-bonded with the N−H proton. A careful look at the $^1$H NMR spectrum shows a small signal near 12 ppm stemming from the minor *Z* configuration. The calculated geometries (B3LYP/6-31G(d, p) level of theory) of the two configurations in $CD_3CN$ showed that the *E* configuration is more stable than *Z*, which is in agreement with the isomer ratio observed in the $^1$H NMR spectrum. The addition of 1.6 equiv of TFA to $CD_3CN$ solutions of **1**-*E*, **2**-*E*, and **3**-*E* protonated the pyridine subunit, which was accompanied by a color change in the solution from light yellow to orange (Figure 3c) and drastic changes in the $^1$H NMR and $^{19}$F NMR spectra (Figure 2).

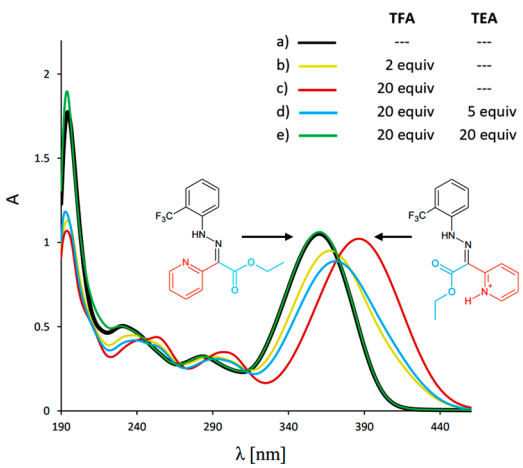


**Figure 3.** Changes in the UV−vis spectrum during the acid/base switching of **1**-*E*. All data were recorded in MeCN at 298 K using a $1.2 \times 10^{-4}$ M solution of **1**-*E*. Spectra a and e are overlapping.

First, the N−H proton signals at 15 ppm disappeared, and new signals appeared at 13 ppm. This shift indicates that rotation around the C=N bond has occurred (*E*/*Z* isomerization) and that the N−H proton formed a hydrogen bond with the carbonyl group of the ester subunit, yielding *Z*-$H^+$. Second, the pyridine proton signals shifted upfield, which is typical for protonated pyridine rings (Figure S9). In the $^{19}$F NMR spectra, peaks from the $-CF_3$ group can be seen near −62.0 ppm. With the addition of TFA, these peaks moved toward higher frequencies for **1**-*E* and **3**-*E*, and those for the **2**-*E* peak moved toward a lower frequency. For the *o*-isomer (**1**-*E*), the greatest change in the chemical shift was −1.8 ppm. The $^{19}$F NMR signals were sharper (8 Hz) than the N−H signals recorded by $^1$H NMR (25 Hz) (width at half the peak height). To better describe the switching process, the *Z*-$H^+$ molar fraction was calculated (based on peak integrals) and plotted against the pH of the solution (Figure 4). It can be

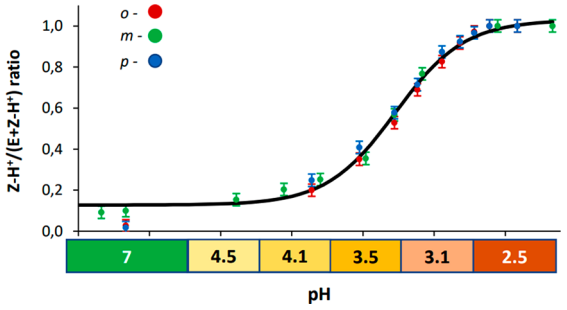


**Figure 4.** Representation of the pH-dependent switching process. Error bars represents standard uncertainy assuming 5% accuracy of the peak integration.

seen that the switching process occurred between pH 4 and 3, and the range is practically identical for all isomers. The relationship from Figure 4 can be used for determination of the pH of a solution. Within the 3−4 range, it is possible with a standard uncertainty of 0.05 pH units. Outside this range, the pH can be estimated as either >4 or <3.



https://doi.org/10.1021/acs.analchem.1c04978
Anal. Chem. 2022, 94, 3427−3431

Upon the addition of 1.6 equiv of triethylamine (TEA) to the $CD_3CN$ solution of $Z$-$H^+$, the color of the solution changed back to light yellow (Figure 3e). The $^1H$ NMR and $^{19}F$ NMR spectra (Figures S9−S11), recorded immediately after the addition of TEA, showed the complete disappearance of $Z$-$H^+$ and the presence of both **1**-*E* and **1**-*Z* in solution. This is evident from the disappearance of the H-bonded N−H peak at 13 ppm and the appearance of two H-bonded N−H peaks (a larger one at 15 ppm and a smaller one at 12 ppm), which were assigned to *E* and *Z*, respectively. In each case, the $T_1$ and $T_2$ relaxation times of the fluorine atom of the *E*- and $Z$-$H^+$ isomers were 1.4−1.6 s and did not change significantly during acidification (Figures S16−S18). Such behavior greatly simplifies the imaging procedure, as only variations of chemical shifts must be taken into account. Since the pH-dependent chemical shift changes are relatively large, the compounds can be used in the MRI of pH gradients. Figure 5 shows the $^{19}F$

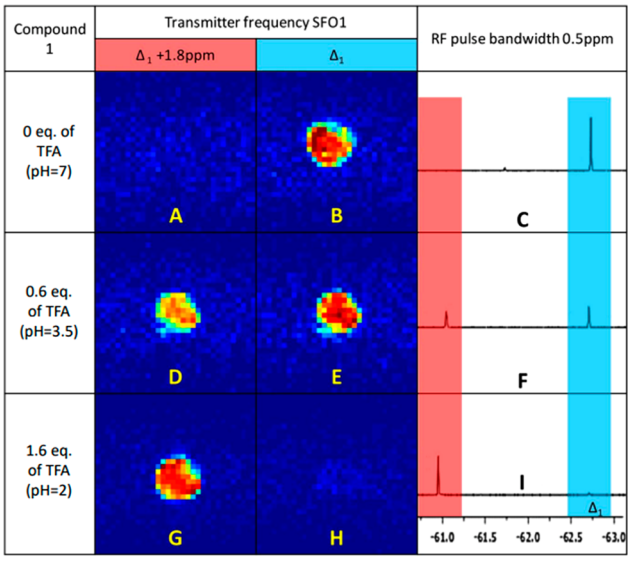


**Figure 5.** $^{19}F$ MRI of compound **1** in $CH_3CN$. (A,D,G) RF excitation pulse at −60.9 ppm with 0.5 ppm bandwidth; (B,E,H) RF excitation pulse at −62.7 ppm with 0.5 ppm bandwidth; (C,F,I) corresponding $^{19}F$ NMR spectra.

MRI images of acetonitrile solutions (15 mM) of **1**, which display the highest impact of pH on the chemical shift of the $CF_3$ functionality. The images were acquired with the appropriate RF excitation pulse frequency and bandwidth of 0.5 ppm to cover the resonance frequencies of the isomers (Figure 5C,E,I). The required acquisition times were 15 min and only 2 min for FLASH and RARE sequences, respectively. We were also able to perform analogous imaging with compound **3** (Figure S15). Unfortunately, the difference in chemical shifts for the isomers of compound **2** (0.1 ppm) turned out to be too small to register good-quality images within a reasonable time. While the chemical shift of the *Z* isomer showed a certain pH dependence (Figures S9−S11), the spectral distance between the $^{19}F$ lines of the *E* and *Z* isomers was large enough to obtain separate images for the entire range of pH values. If necessary, it is possible to increase the RF pulse bandwidth for MR imaging to determine the presence of the *Z* isomer and cover its entire pH-dependent range of chemical shifts.

To explain the differences in the $^{19}F$ NMR chemical shifts for the isomers **1**-*E*, **2**-*E*, and **3**-*E*, we performed DFT calculations to visualize their molecular orbitals. The shape of the orbitals clearly indicates an increased density of electrons in the *o*- and *p*-positions (Table S2), while a much lower density was observed at the *m*-positions. This is due to a mesomeric effect in which the nitrogen of the hydrazone group is an electron donor to the aromatic ring. The distinct range of changes in chemical shifts in the $^{19}F$ NMR spectrum during *E*/*Z* configuration switching in compounds **1**−**3** can be explained based on the differences in the binding energies of the hydrazone hydrogen. For the *E* configuration, the bond was stronger (N−H---N), and for the *Z* configuration, it was weaker (N−H---O).[35] Thus, the stronger bond polarization in the *E* configuration increased the electron-donating properties of the pyridyl nitrogen, which increased the electron density at the *o*- and *p*-positions. The highest change in the chemical shift was coupled with the biggest change in energy during switching for the *o*-isomer, as demonstrated in Figure 6.

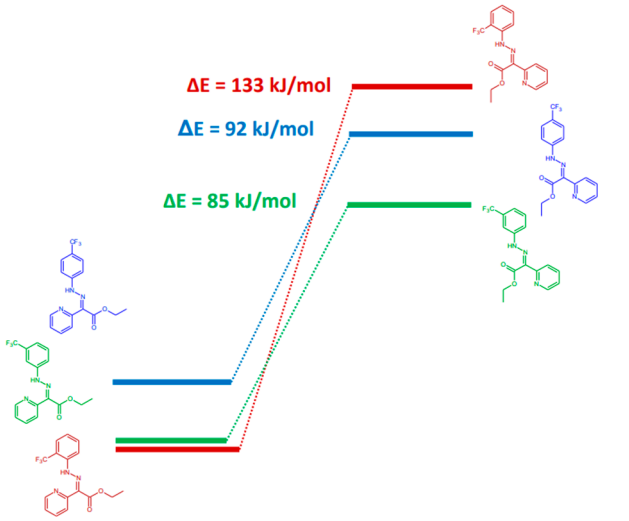


**Figure 6.** Calculated energy diagram for *E*/*Z* configuration changes of compounds **1**, **2**, and **3**.

Additionally, the $-CF_3$ group at the *o*-position was surrounded by strongly electronegative atoms (oxygen or nitrogen), which significantly impacted the magnetic properties of fluorine atoms.

Although the *E* isomers showed poor water solubility, they were highly soluble (>20−40 mg/mL) in polar organic solvents, and their protonated forms ($Z$-$H^+$ isomers) were slightly soluble in water (Table S5). In practical applications for $^{19}F$ MRI in medical diagnostics, insoluble fluoroorganic compounds are typically used as aqueous emulsions.[36] In the case of **1**, we prepared a stable vegetable oil−water emulsion with pluronic-127 as a surfactant. The emulsion showed similar features in $^{19}F$ NMR and $^{19}F$ MRI experiments as the acetonitrile solution, except for higher peak widths of 80 Hz compared with 8 Hz in solution (Figures S19 and S21), which are still comparable to the RF pulse bandwidths used in previous MRI experiments.

In conclusion, we obtained a series of hydrazone molecular switches containing the $-CF_3$ functionality. This allowed the visualization of the switching process by $^{19}F$ NMR, $^1H$ NMR, UV−vis, and $^{19}F$ MRI in the low (millimolar) concentration range with a short acquisition time in both polar organic


https://doi.org/10.1021/acs.analchem.1c04978
Anal. Chem. 2022, 94, 3427−3431

solvents or aqueous emulsions. The chemical shift changes for the **1**-*E* isomer were surprisingly large, which opens possibilities for applications of such molecular switches as smart MRI contrast agents. Further research is currently in progress in our laboratory to tune the pH-switching range and improve their aqueous solubility. The latter should be achieved by the introduction of polyethylene glycol or carbohydrate functionalities.[37]

## ■ ASSOCIATED CONTENT

### Supporting Information

The Supporting Information is available free of charge at https://pubs.acs.org/doi/10.1021/acs.analchem.1c04978.

Chemicals and reagents, measurements, hardware and software configuration, sample preparation, additional experimental details, materials, and methods (PDF)

## ■ AUTHOR INFORMATION


### Corresponding Author

**Tomasz Krawczyk** − *Department of Chemical Organic Technology and Petrochemistry, Silesian University of Technology, 44-100 Gliwice, Poland;* orcid.org/0000-0002-4862-0079; Email: tomasz.krawczyk@posl.pl

### Authors

**Dawid Janasik** − *Department of Chemical Organic Technology and Petrochemistry, Silesian University of Technology, 44-100 Gliwice, Poland*

**Krzysztof Jasiński** − *Institute of Nuclear Physics Polish Academy of Sciences, 31-342 Krakow, Poland*

**Władysław P. Węglarz** − *Institute of Nuclear Physics Polish Academy of Sciences, 31-342 Krakow, Poland*

**Ivan Nemec** − *Central European Institute of Technology Brno University of Technology, 612-00 Brno, Czech Republic; Department of Inorganic Chemistry, Faculty of Science, Palacký University 17, 771 46 Olomouc, Czech Republic*

**Pawel Jewula** − *Central European Institute of Technology Brno University of Technology, 612-00 Brno, Czech Republic*

Complete contact information is available at: https://pubs.acs.org/10.1021/acs.analchem.1c04978


### Author Contributions

Dawid Janasik: methodology, formal analysis, investigation, writing of original draft, visualization. Krzysztof Jasiński: investigation, visualization. Władysław P. Węglarz: methodology. Paweł Jewuła: methodology. Ivan Nemec: investigation. Tomasz Krawczyk: conceptualization, resources, writing of original draft, review and editing.

### Notes

The authors declare no competing financial interest.

## ■ ACKNOWLEDGMENTS

We thank the Silesian University of Technology for financial support.

## ■ DEDICATION

We thank the Silesian University of Technology for the financial support (Grant 04/050/BKM21/0132)

## ■ REFERENCES


(1) Di Costanzo, L.; Panunzi, B. *Molecules* **2021**, *26* (10), 2952.
(2) Monteiro, M. C. O.; Koper, M. T. M. *Curr. Opin. Electrochem.* **2021**, *25*, 100649.
(3) Benitz, W. *Infectious Disease and Pharmacology*; Elsevier, 2019.
(4) Badillo, R. *World J. Gastrointest. Pharmacol. Ther.* **2014**, *5* (3), 105.
(5) Tannock, I. F.; Rotin, D. *Cancer Res.* **1989**, *49* (16), 4373−4384.
(6) Hao, G.; Xu, Z. P.; Li, L. *RSC Adv.* **2018**, *8* (39), 22182−22192.
(7) Li, S.-S.; Zhang, M.; Wang, J.-H.; Yang, F.; Kang, B.; Xu, J.-J.; Chen, H.-Y. *Anal. Chem.* **2019**, *91* (13), 8398−8405.
(8) Zeng, J.; Shirihai, O. S.; Grinstaff, M. W. *JoLS, J. Life Sci.* **2020**, *2* (4), 25−37.
(9) Anemone, A.; Consolino, L.; Arena, F.; Capozza, M.; Longo, D. L. *Cancer Metastasis Rev.* **2019**, *38* (1−2), 25−49.
(10) Pierre, V. C.; Allen, M. J.; Caravan, P. *JBIC J. Biol. Inorg. Chem.* **2014**, *19* (2), 127−131.
(11) Wahsner, J.; Gale, E. M.; Rodríguez-Rodríguez, A.; Caravan, P. *Chem. Rev.* **2019**, *119* (2), 957.
(12) Hequet, E.; Henoumont, C.; Muller, R. N.; Laurent, S. *Future Med. Chem.* **2019**, *11* (10), 1157−1175.
(13) Janasik, D.; Krawczyk, T. *Chem. Eur. J.* **2022**, *28* (5), e202102556.
(14) Peterson, K. L.; Srivastava, K.; Pierre, V. C. *Front. Chem.* **2018**, DOI: 10.3389/fchem.2018.00160.
(15) Deutsch, C. J.; Taylor, J. S. *Ann. N.Y. Acad. Sci.* **1987**, *508*, 33−47.
(16) Frenzel, T.; Koler, S.; Bauer, H.; Niedballa, U.; Weinmann, H. J. *Investigative Radiology* **1994**, *29*, S220−S222.
(17) Metcalfe, J. C.; Hesketh, T. R.; Smith, G. A. *Cell Calcium* **1985**, *6* (1−2), 183−195.
(18) Oishi, M.; Sumitani, S.; Bronich, T. K.; Kabanov, A. V.; Boska, M. D.; Nagasaki, Y. *Chem. Lett.* **2009**, *38* (2), 128−129.
(19) Chen, S.; Yang, Y.; Li, H.; Zhou, X.; Liu, M. *Chem. Commun.* **2014**, *50* (3), 283−285.
(20) Huang, X.; Huang, G.; Zhang, S.; Sagiyama, K.; Togao, O.; Ma, X.; Wang, Y.; Li, Y.; Soesbe, T. C.; Sumer, B. D.; Takahashi, M.; Sherry, A. D.; Gao, J. *Angew. Chemie Int. Ed.* **2013**, *52* (31), 8074−8078.
(21) Li, Y.; Zhang, H.; Guo, C.; Hu, G.; Wang, L. *Anal. Chem.* **2020**, *92* (17), 11739−11746.
(22) Zhang, C.; Li, L.; Han, F. Y.; Yu, X.; Tan, X.; Fu, C.; Xu, Z. P.; Whittaker, A. K. *Small* **2019**, *15* (36), 1902309.
(23) Gianolio, E.; Napolitano, R.; Fedeli, F.; Arena, F.; Aime, S. *Chem. Commun.* **2009**, *40*, 6044.
(24) Bonnet, C. S.; Tóth, É. *Chim. Int. J. Chem.* **2016**, *70* (1), 102−108.
(25) Aprahamian, I. *Chem. Commun.* **2017**, *53* (50), 6674−6684.
(26) Harris, J. D.; Moran, M. J.; Aprahamian, I. *Proc. Natl. Acad. Sci. U. S. A.* **2018**, *115* (38), 9414−9422.
(27) Feringa, B. L. *Molecular Switches*; Wiley VCH, 2001.
(28) Nacci, C.; Baroncini, M.; Credi, A.; Grill, L. *Angew. Chemie Int. Ed.* **2018**, *57* (46), 15034−15039.
(29) Arramel; Pijper, T. C.; Kudernac, T.; Katsonis, N.; van der Maas, M.; Feringa, B. L.; van Wees, B. J. *Nanoscale* **2013**, *5* (19), 9277.
(30) Jerca, V. V.; Hoogenboom, R. *Angew. Chemie Int. Ed.* **2018**, *57* (27), 7945−7947.
(31) Wu, D.; Sedgwick, A. C.; Gunnlaugsson, T.; Akkaya, E. U.; Yoon, J.; James, T. D. *Chem. Soc. Rev.* **2017**, *46* (23), 7105−7123.
(32) Xia, T.; Li, N.; Fang, X. *Annu. Rev. Phys. Chem.* **2013**, *64* (1), 459−480.
(33) Landge, S. M.; Tkatchouk, E.; Benítez, D.; Lanfranchi, D. A.; Elhabiri, M.; Goddard, W. A.; Aprahamian, I. *J. Am. Chem. Soc.* **2011**, *133* (25), 9812−9823.
(34) Su, X.; Lessing, T.; Aprahamian, I. *Beilstein J. Org. Chem.* **2012**, *8*, 872−876.
(35) Su, X.; Lõkov, M.; Kütt, A.; Leito, I.; Aprahamian, I. *Chem. Commun.* **2012**, *48* (85), 10490.
(36) Wu, L.; Liu, F.; Liu, S.; Xu, X.; Liu, Z.; Sun, X. *Int. J. Nanomedicine* **2020**, *15*, 7377−7395.

(37) Yu, M.; Bouley, B. S.; Xie, D.; Que, E. L. *Dalt. Trans.* **2019**, *48* (25), 9337−9341.



https://doi.org/10.1021/acs.analchem.1c04978
*Anal. Chem.* 2022, 94, 3427−3431